



## ARTICLE

# Design, fabrication, and characterization of a multimodal reconfigurable bioreactor for bone tissue engineering

Margherita Montorsi<sup>1,2</sup>  | Giada G. Genchi<sup>1</sup> | Daniele De Pasquale<sup>1</sup> |  
Giorgio De Simoni<sup>3</sup> | Edoardo Sinibaldi<sup>4</sup> | Gianni Ciofani<sup>1</sup> 

<sup>1</sup>Istituto Italiano di Tecnologia, Smart Bio-Interfaces, Pontedera, Italy

<sup>2</sup>Scuola Superiore Sant'Anna, The BioRobotics Institute, Pontedera, Italy

<sup>3</sup>CNR, Nanoscience Institute, NEST Laboratory, Pisa, Italy

<sup>4</sup>Istituto Italiano di Tecnologia, Bioinspired Soft Robotics, Genova, Italy

## Correspondence

Margherita Montorsi and Gianni Ciofani, Istituto Italiano di Tecnologia, Smart Bio-Interfaces, Viale Rinaldo Piaggio 34, 56025 Pontedera, Italy.

Email: [margherita.montorsi@iit.it](mailto:margherita.montorsi@iit.it) and [gianni.ciofani@iit.it](mailto:gianni.ciofani@iit.it)

## Abstract

In the past decades, bone tissue engineering developed and exploited many typologies of bioreactors, which, besides providing proper culture conditions, aimed at integrating those bio-physical stimulations that cells experience in vivo, to promote osteogenic differentiation. Nevertheless, the highly challenging combination and deployment of many stimulation systems into a single bioreactor led to the generation of several unimodal bioreactors, investigating one or at mostly two of the required biophysical stimuli. These systems miss the physiological mimicry of bone cells environment, and often produced contrasting results, thus making the knowledge of bone mechanotransduction fragmented and often inconsistent. To overcome this issue, in this study we developed a perfusion and electroactive-vibrational reconfigurable stimulation bioreactor to investigate the differentiation of SaOS-2 bone-derived cells, hosting a piezoelectric nanocomposite membrane as cell culture substrate. This multimodal perfusion bioreactor is designed based on a numerical (finite element) model aimed at assessing the possibility to induce membrane nano-scaled vibrations (with ~12 nm amplitude at a frequency of 939 kHz) during perfusion (featuring 1.46 dyn cm<sup>-2</sup> wall shear stress), large enough for inducing a physiologically-relevant electric output (in the order of 10 mV on average) on the membrane surface. This study explored the effects of different stimuli individually, enabling to switch on one stimulation at a time, and then to combine them to induce a faster bone matrix deposition rate. Biological results demonstrate that the multimodal configuration is the most effective in inducing SaOS-2 cell differentiation, leading to 20-fold higher collagen deposition compared to static cultures, and to 1.6- and 1.2-fold higher deposition than the perfused- or vibrated-only cultures. These promising results can provide tissue engineering scientists with a comprehensive and biomimetic stimulation platform for a better understanding of mechanotransduction phenomena beyond cells differentiation.

## KEYWORDS

biomimetic stimulations, bone tissue engineering, multimodal bioreactor, reconfigurability

This is an open access article under the terms of the Creative Commons Attribution-NonCommercial-NoDerivs License, which permits use and distribution in any medium, provided the original work is properly cited, the use is non-commercial and no modifications or adaptations are made.

© 2022 The Authors. *Biotechnology and Bioengineering* published by Wiley Periodicals LLC.

## 1 | INTRODUCTION

Critical size skeletal defects resulting from trauma, tumor, or pathological disorders typically require the use of bone grafts, both of human and animal origin. However, bone grafting procedures are restricted by the limited availability of bone that can be harvested from the iliac crest, and by the expensive medical complications that may be following tissue harvesting.

To face these issues, bone tissue engineering (BTE) has emerged as alternative therapeutic strategy (Braddock et al., 2001), as it could generate unlimited amounts of viable tissue substitutes, involving three main components: (1) an osteo-competent cell source, (2) a compliant biomaterial as a scaffold, and (3) a proper biochemical and biophysical stimulation *in vitro* to allow for cell differentiation (Martin et al., 2004). This innovative engineering approach leverages on bioreactors, that biologists can use to culture cells on scaffolds under proper culture conditions, while efficient cell nutrition is ensured by continuously mixing media and by the convective transport of nutrients (Navarro et al., 2019). Beside the biochemical stimulation—normally achieved through differentiating factors such as ascorbic acid (AA), dexamethasone (DEX), and  $\beta$ -glycerophosphate ( $\beta$ -GP) (Coelho & Fernandes, 2000; Genchi et al., 2016; Marino et al., 2014)—it is also highly desirable that the bioreactors properly mimic *in vitro* the biophysical inputs experienced by bone cells *in vivo*, and namely: (1) the hydrodynamic shear stress, resulting from interstitial fluid movement (from 8 to 30 dyn/cm<sup>2</sup>) (Hadida & Marchat, 2020; McCoy & O'Brien, 2010), (2) the micromechanical strain caused by bending and compression during physical activity (estimated values <2000  $\mu\epsilon$ ) (McCoy & O'Brien, 2010), and (3) the electric impulse that can arise from the bone matrix itself due to the intrinsic piezoelectricity of its components (Genchi et al., 2016; Marino et al., 2014; Sladkova & de Peppo, 2014). Both biochemical and biophysical inputs are indeed critical for the activation of certain genetic pathways, inducing cells to develop a bone phenotype. It has been demonstrated that, for example,  $\beta$ -GP serves as a phosphate source for bone mineral and induces osteogenic gene expression by extracellular related kinase phosphorylation, while DEX induces Runx2 expression by LIM-domain protein (FHL2)/ $\beta$ -catenin-mediated transcriptional activation, and enhances Runx2 activity by upregulation of TAZ (transcriptional coactivator with PDZ-binding motif) and MKP1 (a component of the mitogen-activated protein kinase [MAPK] signaling pathway) (Langenbach & Handschel, 2013). In the same way, the application of external physical *stimuli* regulate stretch-activated ion channels and integrin-initiated cytoskeleton deformations, and ultimately culminates in the activation of genes involved in the differentiation process (Katsumi et al., 2004; Stewart et al., 2020).

The influence of shear stress on bone tissue functional development has widely been investigated over the past decade, leading to various experimental setups, that is, parallel plate flow chambers, rotating disc or radial flow devices, cone and plate viscometers, jet impingement systems, and microfluidic apparatuses (Goldstein et al., 2001; Ingber et al., 2021; Ponomarenko, 2016; Yeatts & Fisher, 2011).

Osteogenesis controlling through mechanical means has already been demonstrated through several methods, including passive and active means. Passive methods are based on altering cell substrate topography and stiffness (Dalby et al., 2008; Kilian et al., 2010; Marino et al., 2014), while active methods include exposure to variation of forces from external sources—as centrifugal (Prodanov et al., 2013), vibrational (Campsie et al., 2019; Curtis et al., 2013; Kim et al., 2012; Nikukar et al., 2013; Pemberton, 2015), Hydrostatic, and compressive force (B. Liu et al., 2021; J. Liu et al., 2009), or through ultrasonic pressure waves at various frequencies (Chiu et al., 2015; Genchi et al., 2018; Suzuki et al., 2009; Uddin & Qin, 2013). Results of these studies provided a growing understanding that physical stimulation of the cells at a microscale or nanoscale level can greatly enhance osteo-competent cell differentiation.

Along with mechanical stimulations, electrical stimulations have also been studied to promote bone regeneration, and it is currently administered by using three different approaches: direct current (DC) (Khaw et al., 2021; Srirussamee et al., 2021; Y. Zhang et al., 2021), pulsed electromagnetic field (PEMF) (Benya et al., 2021; Diniz et al., 2002; Dong et al., 2021), and capacitive coupled (CC) (Chalidis et al., 2011). The main problems affecting the application of these methods *in vitro* are due to the lack of standardization of cell types, models and protocols, the high risk of contamination, and the invasiveness and high costs of the surgical procedures that would follow *in vivo* (Bhavsar et al., 2020). To overcome these issues, scientific community started to look with increasing interest at piezoelectric materials, as they can create an electric field without the need of external wires—invasive and carriers of possible contamination—and that can be restricted to a certain region of the living tissue. In other words, piezoelectric biomaterials can represent electroactive implantable interfaces for wireless electrical stimulation delivery, activated thanks to simple environmental stimuli (mechanical waves such as sounds or ultrasounds, US) (Ciofani et al., 2013). Many different piezoelectric materials have been tested as substrates to promote osteoregeneration. Among these materials, some piezoelectric fluoropolymers, like poly(vinylidenedifluoride) (PVDF) (Ribeiro et al., 2015) and its copolymer with trifluoroethylene P(VDF-TrFE), have been found to be highly biocompatible and easily processable, exhibiting even improved mechanical and piezoelectric properties suitable to bone repair/regeneration when doped with other ceramic piezoelectric nanomaterials as boron nitrite nanotubes (BN-NTs) or barium titanate nanoparticles (BT-NPs) (Genchi et al., 2016, 2018). BT is a well-known dielectric ceramic with piezoelectric coefficients of 90 and 190 pC/N along the [001] and [111] directions of the perovskite crystal. BT is a promising nucleating filler for PVDF-based composites due to its easy preparation via a procedure that allows for the precise control of their shape and morphology. Other advantages include its high piezoelectric coefficient, scalable and low-cost processing, and biocompatibility as a lead-free material. Membranes and films composed of PVDF-TrFE and BT nanostructures have been effectively utilized in a number of studies to enhance osteoblast-like cell differentiation (Surmenev et al., 2019), to precondition cells *in vitro* before

implantation of the cell/scaffold construct *in vivo*, or to recruit cells once the biomaterial is grafted into the bone defect (X. Zhang et al., 2016). There are in fact evidence that the surface potential of polarized PVDF-TrFE/BT-NPs membrane reaches  $-76.8$  mV, which is in the range of natural endogenous biopotential; the stability of the achieved potential is also remarkable, having a half-life of 12 weeks when implanted in bone defects (X. Zhang et al., 2016).

The complexity of implementing all of the abovementioned inputs and stimulation sources into a single integrated device, along with the difficulties of controlling them individually and with an incomplete understanding of mechanotransduction phenomena, has motivated the development of several unimodal/bimodal stimulation devices that ensure one or two stimulation sources (Choi et al., 2019; Liu et al., 2021; Ravichandran et al., 2018; Teoh et al., 2021), therefore poorly mimicking physiological bone environment.

Another important issue related to bioreactors in BTE is the lack of uniformity between each developed stimulation device. Differences in the bioreactor culture chamber geometry, scaffold material and size, type of exploited physical stimuli, and type of cell line used in experiments complicate the understanding of osteodifferentiation processes (Castro, Ribeiro, et al., 2020; Meneses et al., 2020; Rangarajan et al., 2014; Van Dyke et al., 2012). BTE lacks of a comprehensive knowledge, and culminates in the growth of partial information that does not consider fundamental parameters of bone tissue regeneration—like the presence of different correlated biophysical inputs—thus hampering the possibility to draw conclusive statements from the related observations.

In an attempt to overcome these limitations, the present work aimed at designing, modeling, fabricating, and testing a perfusion and ultrasound-driven nano-vibrational, reconfigurable bioreactor for bone-derived cell culture, based on a piezoelectric P(VDF-TrFE)/BTNPs nanocomposite membrane as a cell culture substrate, designed to generate an electric voltage on its surface of  $\sim 10$  mV. Our device enabled the investigation of the effects of each osteodifferentiation-relevant stimulation independently, and at evaluating synergic effects of multiple stimulations in terms of osteogenic response.

Concerning bioreactor design, we exploited numerical simulations (both for the involved fluid-dynamic and ultrasonic fields) to instruct the fabrication of the device, before prototyping. Once prototyped, we used the proposed bioreactor to investigate four different configurations, namely: (1) a static configuration (no stimuli, as control), (2) a plain perfusion configuration (flow only, no ultrasound), (3) a vibration-activated piezoelectric configuration (ultrasound only, no flow), and (4) a multimodal configuration (including flow and ultrasound), as perfusion synergic with vibration-activated piezoelectric stimulations. Effects of the different cultural configurations were assessed in terms of inorganic and organic matrix deposition by cytochemistry, immunocytochemistry, and optical microscopy.

We found that the application of multiple biomimetic physical stimulations in combination with differentiative biochemical conditions led to faster cell differentiation, resulting in more abundant

matrix protein deposition with respect to the unimodal/bimodal counterparts, and to even a higher extent with respect to the plain biochemical stimulation, corroborating evidence on mechanotransduction as a fundamental actor in the osteodifferentiation bioprocess. Our multimodal bioreactor could be therefore exploited to easily and more quickly pre-condition cells on the piezoelectric biocompatible membrane, before its *in vivo* grafting to the site of injury, thus resulting in faster and more effective tissue regeneration.

## 2 | MATERIALS AND METHODS

### 2.1 | P(VDF-TrFE)/BTNP membrane fabrication

Based on previous work from our group (Genchi et al., 2016), we fabricated a nanocomposite piezoelectric membrane by dispersing tetragonal crystalline barium titanate nanoparticles ( $\text{BaTiO}_3$  NPs, BTNPs from NanoAmor,  $\sim 300$  nm size) in a polymeric matrix of P(VDF-TrFE) (Piezotech, 70/30% mol copolymer). Briefly, 0.8 g of P(VDF-TrFE) were dissolved in 10 ml of methyl ethyl ketone and sonicated for 3 min with a Branson sonicator set at 8 W; then, 1.2 g of BTNPs were added and sonicated for other 3 min, until the 40% P(VDF-TrFE)/60% BTNP (w/w) mixture resulted visually homogenous. The mixture was allowed to rest for 1 day before further processing. Membranes were obtained by casting of 800  $\mu\text{l}$  of mixture on Ibidi film pieces (28 mm  $\times$  70 mm), and by annealing at  $+50^\circ\text{C}$  on a hot plate for 4 h. Complete solvent evaporation was allowed by placing membranes under vacuum overnight. Then, samples were exposed to  $\text{O}_2$  plasma (25 sccm, 50 W, 120 s, 0.5 mbar) to increase surface hydrophilicity and facilitate the absorption of medium proteins before cell seeding.

### 2.2 | Bioreactor design

A bicompartmental bioreactor was designed with Solidworks 2020 software upon verification of the membrane biocompatibility (see Figures S1–S3, for details). Inspired by some examples of parallel-plates flow chamber (PPFC) bioreactors presented in the literature (Grillone et al., 2019; Kreke et al., 2005, 2008; McCoy & O'Brien, 2010; Scaglione et al., 2008), our system was characterized by a top plastic channel hosting a laminar flow, separated from a static silicon-based bottom compartment by a piezoelectric membrane suspended over a rectangular window. The upper channel, or “fluid dynamic channel” for nutrients supply and shear stress development, was designed to guarantee a wall shear stress (WSS) in the range of that one identified in the relevant literature for osteoinduction tests ( $0.01$ – $20$  dyn/cm<sup>2</sup>) (Fernandez-Yague et al., 2015). The bottom compartment was also designed with an inlet for an immersion probe able to deliver (only when required) a 2.6 W planar wave of low-intensity pulsed ultrasounds (LIPUS) through an ultrasound generator (SonoPore KTAC-4000 from Nepagene). This experimental configuration was expected to

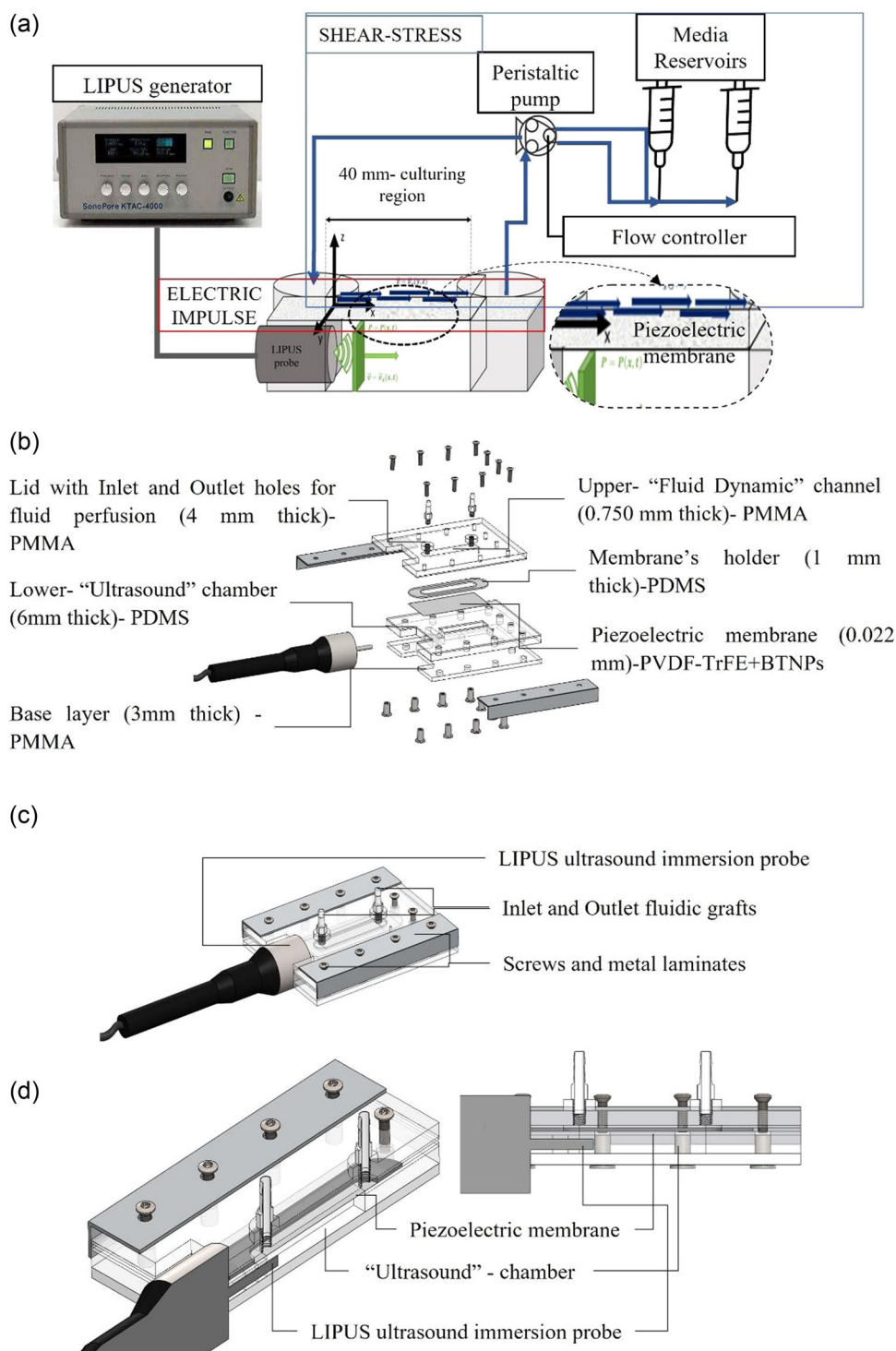


**FIGURE 1** (a) Scheme of the multimodal stimulating apparatus. (b) Computer assisted design of the multimodal bioreactor by Solidworks software; exploded view representing the multilayered structure holding the P(VDF-TrFe)/BTNP membrane in the middle. (c) Sealed bioreactor compacted by metal profiles, integrated with the US probe and fluidic inlets. (d) Cross sectional view of the sealed bioreactor, highlighting the relative position between the US probe and the P(VDF-TrFe)/BTNP membrane. BTNP, barium titanatenanoparticles; LIPUS, low-intensity pulsed ultrasounds; PDMS, polydimethylsiloxane; PMMA, polymethyl methacrylate; P(VDF-TrFe), poly(vinylidene fluoride-co-trifluoroethylene)

produce a hydrodynamic shear stress due to laminar flow and ultrasound-induced vibrational motion on the piezoelectric membrane separating the two compartments, as well as membrane polarization due direct piezoelectric effect (Figure 1a). The

bioreactor was thus a multi-layered structure (Figure 1b), the sealing of which was ensured by 10 screws and self-locking flange bolts pressing on two L-shaped aluminum profiles to distribute the pressure (Figure 1c).

### 2.3 | Fluid dynamic and mechano-acoustic simulation

To simulate the fluid dynamic environment of the bioreactor top compartment and validate the designed sizes of this latter before prototyping, COMSOL Multiphysics software was used. Assuming flow to be laminar and completely developed along the  $x$ -axis, with no slip condition at the compartment walls, the inlet flowrate ( $Q_i$ ) was varied from 5 to 15 ml min<sup>-1</sup> (inlet flowrate in the cylindrical graft) to evaluate fluid flow profile in the range of that one fed to analytical computation (10 ml min<sup>-1</sup>; details of computation are specified in the Results paragraph). Outlet condition was maintained as  $P|_{\text{out}} = 0$  Pa (outlet pressure), the flowing material (cell culture medium: density 993 kg m<sup>-3</sup> and viscosity  $8.9 \times 10^{-4}$  Pa s) was considered as an incompressible and Newtonian fluid, and the channel height was fixed as  $h = 0.750$  mm. The fluid dynamic domain was then defined by a mesh of tetrahedral finite elements and spatial velocity distributions inside the culture micrometric channel were computed.

The same finite element method (FEM) software was used to simulate the mechano-acoustic domain in the bottom compartment. The simulation was performed to ensure that the power supplied by the available LIPUS-probe was sufficient to induce the sought vibration of the piezoelectric membrane (namely a vibration amplitude large enough for inducing a corresponding voltage in the order of 10 mV).

To set up the FEM model boundary condition of the mechano-acoustic domain, that is the normal acceleration of the ultrasonic source, LIPUS probe tip velocity at its maximum power was measured by laser Doppler vibrometry (Figure S4). Upon quantification of the tip harmonic displacement ( $D_{\text{tip}} = 75$  nm) at the probe resonance frequency ( $f_r = 939$  kHz), the effective value of harmonic acceleration was computed as  $a_{\text{eff}} = 2.82 \times 10^6$  m s<sup>-2</sup>. This boundary parameter—along with the acoustic impedance of the bottom polydimethylsiloxane (PDMS) compartment walls, implying  $Z_{\text{PDMS}} = 1.129 \times 10^6$  kg s<sup>-1</sup> m<sup>-2</sup> (Cafarelli et al., 2017)—enabled the simulation of the ultrasonic pressure wave inducing membrane vibration. The domain was again mapped through a tetrahedral finite element mesh, fine enough to resolve the micrometric membrane.

### 2.4 | Reconfigurable bioreactor fabrication

Based on the obtained numerical results, the bioreactor was prototyped by overlap of several layers, fabricated by laser cutting of plastic foils of specific thickness and by silicone casting on/removal from 3D printed molds, followed by UV irradiation for sterilization.

More precisely, for the fabrication of the bioreactor fluid dynamic compartment, a polymethyl methacrylate (PMMA) transparent sheet with a 0.750 mm thickness was laser-cut with high resolution Versa-Laser cutter (Universal Laser System operated at 100% power, 100% speed), and then glued irreversibly to a lid. The same fabrication approach was used for the lid and the basement

layer. Briefly, the lid was obtained by a 4-mm-thick PMMA sheet laser cut to obtain 10 bolt holes (diameter  $\varphi = 3$  mm) for sealing of the bioreactor, a bubble venting hole, and flow inlet and outlet holes ( $\varphi = 5$  mm). The basement was obtained by a 3-mm-thick PMMA sheet cut to carry 10 nut holes ( $\varphi = 5$  mm). The threading of the holes was hand-made with a suitable tool.

The fabrication of the bioreactor silicon static compartment in PDMS first required the development of a “mold box” for pouring of the silicon and imparting the desired shapes to it. The mold was obtained through a 3D printing rapid prototyping technology, and featured two interconnected cavities and a lateral hole. These cavities were designed to dissipate US-probe heating and for bottom compartment degassing. The PDMS mixture (base to curing agent weight ratio of 1:10) was then poured into the mold box, and curing was allowed at room temperature for 24 h (Figure S5). A 1 mm thick PDMS mask was developed to cover the heat dissipation chamber and the venting channel of the bottom compartment. To secure the membrane at the upper fluid dynamic channel, a 1-mm PDMS holder was fabricated and treated with oxygen plasma for 15 min at 100 W. O<sub>2</sub>-plasma processing reversibly anchored the PDMS holder both to the PMMA layer and to the membrane, thus ensuring the watertightness of the compartment.

To assess the heating effect of the ultrasonic stimulation, bioreactor temperature in the electroactive-vibrational configuration (without medium flow) and in the multimodal configuration (with medium flow) were monitored by an immersion sensor, both in the top cell-laden chamber and in the lower phosphate-buffered saline (PBS) filled compartment. Bioreactors were maintained in the incubator environment at 37°C during monitoring to replicate experimental conditions.

### 2.5 | Differentiation studies under dynamic cell culture conditions

The enhancing effect of biophysical stimulations on osteogenic differentiation with respect to the simple biochemical osteoinduction was assessed by operating the bioreactor in four different configurations: (1) a static configuration without either medium flow or ultrasounds acting on cell cultures, but just supplying chemical differentiating factors; (2) a perfusion configuration with only differentiating medium flow acting on cell cultures; (3) an electroactive-vibrational configuration with only ultrasounds acting on the bottom of the piezoelectric membrane, with cells under differentiative static conditions; (4) a multimodal configuration implementing both differentiative medium perfusion and electro-mechanical stimulation. After UV irradiation of bioreactor components for 20 min on each side, biological investigations were conducted with the human osteosarcoma SaOS-2 cell line (European Collection of Authenticated Cell Lines 89050205). First, cells were seeded into the bioreactor top compartment (also identified as culture chamber) at a density of 20,000 cells cm<sup>-2</sup>, and cell adhesion was allowed for 48 h under proliferative medium. The latter was



composed of high glucose (4.5 g L<sup>-1</sup>) Dulbecco's modified Eagle's medium (DMEM; Gibco) supplemented with 10% fetal bovine serum (FBS; Sigma F4135), 2 mM L-glutamine (Sigma G7513), 100 U penicillin/100 µg ml<sup>-1</sup> streptomycin (Sigma P4333), and 2.5 µg ml<sup>-1</sup> amphotericin B (Sigma A2942). Then, differentiation was induced by administration low glucose (0.1 g L<sup>-1</sup>) DMEM (Gibco), supplemented with 10% FBS, 10 mM β-glycerophosphate, 100 nM dexamethasone, 50 µM ascorbic acid, 2 mM L-glutamine, and antimicrobials. Based on the previously reported FEM simulation of fluid dynamic and acoustic osteoinductive stimulations, a flowrate of 10 ml min<sup>-1</sup> was applied with an Ibidi pumping system, whereas US were delivered to the cultures daily by applying the following parameters: 2.6 W power, 939 kHz frequency, 20% duty cycle, and 0.5 Hz burst-rate, for 30 min over a period of 7 days.

## 2.6 | Evaluation of the osteodifferentiation

Osteodifferentiation on the PVDF-TrFE/BTNP membranes was quantified by evaluation of the secretion of an organic bone extracellular matrix component, collagen-1 (Col1α1), after 7 days of cell culture in each bioreactor configuration. To the purpose, bioreactors were disassembled, membranes were recovered and immunocytochemistry was performed. First, cells were fixed with 4% paraformaldehyde solution in PBS with calcium and magnesium for 20 min at +4°C. Cells were then permeabilized with a 0.1% Triton™ X-100 (Sigma 93443) solution in 10% goat serum (GS, Sigma G9023) in PBS for 20 min at room temperature. Thereafter, cultures were incubated with a rabbit primary polyclonal anti-collagen type I antibody (Millipore ABT123, 1:100 v/v-diluted in 10% GS) at 37°C for 1 h. After three PBS rinses (5 min each), cells were incubated with a goat secondary TRITC-conjugated anti-rabbit antibody (Invitrogen T2769, 1:100 v/v-diluted in 10% GS) for 1 h at 37°C. Cells were finally rinsed three times with PBS, and four fluorescence microscopy images for each configuration were captured at ×10 magnification with a Nikon C2s confocal microscope. Quantification of the collagen-covered areas was performed by ImageJ image analysis software (freely downloadable from <https://imagej.nih.gov/ij/>), and data were reported by normalization to total image area.

Osteodifferentiation on the PVDF-TrFE/BTNP membranes was also quantified by evaluation of inorganic bone extracellular matrix deposition after 7 days of cell culture in each bioreactor configuration. To the purpose, cell cultures were fixed as previously described, and calcium deposits were stained by incubation with Alizarin Red-S (ALZ; Millipore 2003999) for 1 h at room temperature. Excess dye was removed by thorough washing with distilled water. The stained samples were then imaged by using an optical microscope (Seika Machinery Hirox KH-7700); for each bioreactor configuration, four images were collected. Evaluation of the mineralization was performed by ImageJ image analysis software, and data were reported by normalization to total image area.

Alizarin Red-S based quantification of calcium deposition was then performed as described elsewhere (Zeuner et al., 2018). Briefly,

samples were immersed in 400 µl of 10% acetic acid and incubated under shaking for 30 min at room temperature, and then heated to 85°C for 20 min. Subsequently, the samples were centrifuged at 20,000g for 15 min and the supernatant was transferred to a new test tube. Before the measurement, the pH value was set to 4.3 and the optical density was measured at a wavelength of 405 nm using a spectrophotometer (Perkin Elmer Victor X3).

## 2.7 | Statistical analysis

All experiments were conducted in duplicate for each experimental class; technical replicates were three. All data were imported into R-software to perform statistical analysis. Quantitative data were plotted as mean ± standard deviation (SD). Statistical analysis was performed by using a two samples Student's *t* test. Differences were indicated to be statistically significant when \**p* < 0.05, \*\**p* < 0.01, or \*\*\**p* < 0.001.

## 3 | RESULTS

### 3.1 | Fluid dynamic simulation

Through fluid dynamic numerical simulation we evaluated the velocity spatial distributions (Figure 2a) at different inlet flowrate inside the cells culture chamber (Figure 2b), having fixed the channel height (*h*) at 0.750 mm. The channel height was chosen as fixed parameter in the evaluation of the WSS according to the following analytical reasoning. Under laminar and stationary flow hypothesis, between two parallel plates (distant *h* from each other and characterized by certain width *w* and length *l*, with *l* ≫ *w* ≫ *h*), the WSS assumed the following well known expression (Equation 1) (Grillone et al., 2019):

$$WSS = \frac{6\mu}{h} \langle v \rangle, \quad (1)$$

where  $\langle v \rangle$  is the average fluid velocity along the principal direction and it depends on the flowrate at the inlet ( $Q_i$ ) of the chamber, as well as on the sizes on the flow chamber *h* and *w* (Equation 2):

$$\langle v \rangle = \frac{Q_i}{h \cdot w}. \quad (2)$$

By imposing a channel height *h* = 0.750 mm, with a 10 mm width (*w*) and a 40 mm length (*l*), with a flowrate of  $Q_i = 10 \text{ ml min}^{-1} = 1.66 \times 10^{-7} \text{ m}^3 \text{ s}^{-1}$ , the average fluid velocity in the rectangular duct analytically resulted to be  $\langle v \rangle = 2.2 \times 10^{-2} \text{ m s}^{-1}$ . Finally, wall shear stress resulted to be  $WSS = 1.58 \text{ dyn cm}^{-2}$ , a value which falls in the suitable range for cell stimulation. Numerical FEM simulations at different inlet flow-rate in the range of  $10 \text{ ml min}^{-1}$  (Video S1), confirmed analytical results, and the WSS assumed eligible biomimetic value for all the tested inlet flowrate (Figure 2c). Precisely, with an inlet flowrate of  $10 \text{ ml min}^{-1}$ , the wall shear stress numerically

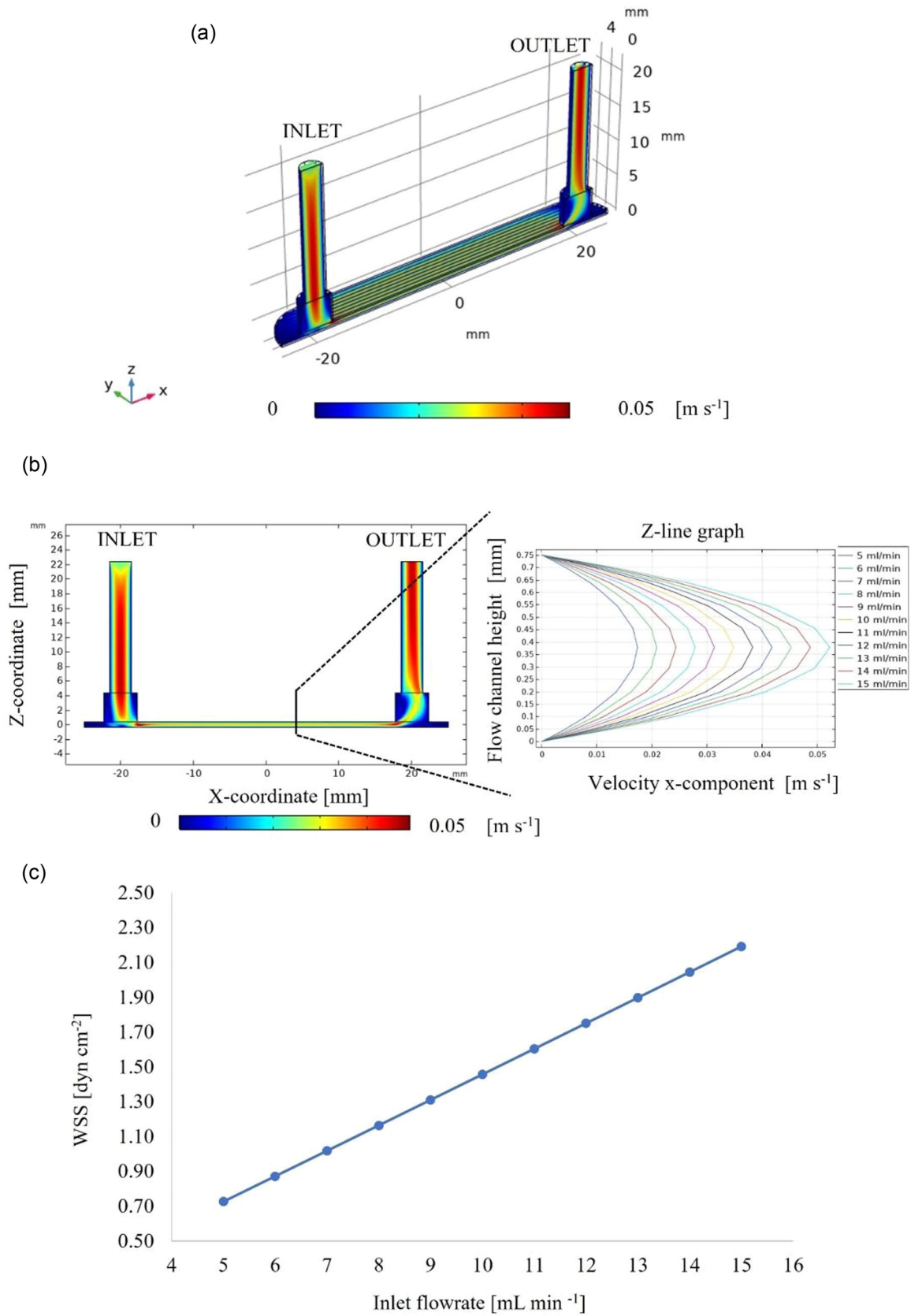


FIGURE 2 (See caption on next page)

resulted as  $WSS = 1.46 \text{ dyn cm}^{-2}$ , that is high enough to stimulate cells osteodifferentiation without occurring in cells detachment from substrate (Hadida & Marchat, 2020).

### 3.2 | Acoustic pressure simulation

The acoustic simulation (Figure 3a) allowed to evaluate the displacement field along the piezoelectric membrane under action of ultrasonic pressure. Membrane vibration in the z-direction ranged from  $-12.6 \text{ nm}$  to  $+12.6 \text{ nm}$  (Figure 3b), and it was well distributed along the membrane, thus also ensuring a relatively homogeneous spatial distribution of the stimulation. As specified in the previous paragraph, the mechanical pressure input is transduced into an electrical output by the piezoelectric membrane. By applying a linear piezoelectric relation between differential pressure and voltage generation on the membrane surface, detailed elsewhere (Marino et al., 2017) and reported in the following as Equation (3):

$$\Delta V = g_{31} \cdot \Delta P \cdot \text{thickness}, \quad (3)$$

and by assuming piezoelectric coefficient  $g_{31} = 0.24 \text{ V mN}^{-1}$  (Genchi et al., 2018) and membrane thickness  $22 \text{ }\mu\text{m}$  (average value actually measured by optical profilometry with a Leica DCM 3D device), the electric impulse that affected cell culture through the designed multimodal device was finally computed and resulted of  $\sim 10 \text{ mV}$  on average on the membrane surface (Figure 3c). These results suggest the potentiality of our stimulation device as a multimodal bioreactor for evaluating the physical environment that can strongly promote the osteogenic differentiation process

### 3.3 | Multimodal bioreactor assembly and characterization

Bioreactor assembly is shown in Figure 4a–c. Thanks to its small footprint and compatibility with cell culturing procedures, the stimulation system could be placed inside an incubator with controlled temperature and humidity without any impact on cell viability, differentiation, and optical monitoring.

Upon filling of the bioreactor compartments with PBS, the membrane was vibrationally characterized by laser Doppler vibrometry in two selected points (Figure 4d). More precisely, membrane vibrations were investigated in close proximity to and far from the US-probe tip (0.2 and 4 cm, respectively, from US source). From the first power spectrum, we found  $D_{\text{MAX-NEAR}} = 1.05 \text{ nm}$ , and the root

mean square (RMS) resulted to be  $D_{\text{rms-NEAR}} = 3 \text{ nm}$ . From the far spectrum, the maximum value resulted  $D_{\text{MAX-FAR}} = 0.91 \text{ nm}$ , while the RMS value was  $D_{\text{rms-FAR}} = 1.45 \text{ nm}$  (Figure 4e). Simulation results and vibrational experimental measurements were thus in agreement, corroborating the model-based design of the bioreactor.

Concerning heating effects, in the electroactive-vibrational configuration, after 30 min of ultrasonic stimulation at  $2.6 \text{ W}$ , temperature increment in the top chamber was about  $2^\circ\text{C}$ , while lower chamber  $3.5^\circ\text{C}$ . When the fluid flow was active, in the multimodal configuration, temperature in the upper chamber underwent an increment of  $1.5^\circ\text{C}$ , while in the lower chamber of  $3^\circ\text{C}$ . All these values, for the duration of the stimulation, are indeed really unlikely to induce any relevant biological effect.

### 3.4 | Osteodifferentiation

Col1 $\alpha$ 1 immunofluorescence staining demonstrated that SaOS-2 cell osteogenic differentiation was improved by the multimodal stimulation with respect to static culture and single/double stimulation (Figure 5a). COL-1 covered area in the multimodal configuration indeed resulted almost 20-fold higher than that one of static cultures, and it was found to be 1.6 and 1.2 higher than that one of the perfusion and vibrational bioreactor configurations, respectively (Figure 5b). These results proved that synergic physical stimulation enhanced osteodifferentiation, and suggest the potentialities of our novel device for a deeper understanding of the mechanotransduction phenomena in bone regeneration.

Alizarin red staining for mineral deposition quantification was found to be coherent to COL-1 labeling (Figure 5c). Cells cultured under multimodal and electroactive-vibrational stimulation were characterized by significantly larger calcium deposits than static cultures, with Alizarin red-positive deposits covering 7.3% and the 9.4% of the total imaged samples area. We suggested that part of the mineral deposits on the multimodal stimulated membrane and on the perfused one may have been lost during stimulation due to the wall shear stress. Indeed, modest staining was seen in cells plated on perfusion sample, but still to a lesser extent on static one—3.7% and 0.7%, respectively (Figure 5d). Levels of mineralization was then quantified by measuring the absorbance of Alizarin Red-S through spectrophotometry (Figure 5e), after dye recovery from samples. Results confirmed data obtained from image analysis: cells subjected to the electroactive-vibrational configuration showed the overall highest level of mineralization with respect to all other groups, with an absorbance value of 0.13 a.u. against 0.9 a.u. of the static one.

**FIGURE 2** Fluid dynamic simulation of the upper flow chamber. The symmetry of the domain allows to consider just half of the chamber thus reducing the computational weight of the simulation. (a) Velocity field in the flow chamber represented by parallel XZ streamlines. Inlet and outlet conditions was set as:  $Q_i = 10 \text{ ml min}^{-1}$ ;  $P_o = 0 \text{ Pa}$ . (b) XZ-plane streamline at  $y = 0$  (plane of symmetry): the X-component of velocity  $U_x(z)$  is assumed to develop the well-know parabolic trend along channel height. (c) Wall shear stress (WSS) above the piezoelectric membrane at different inlet flowrate. The designed culture chamber sizes—thickness  $0.750 \text{ mm}$  and width  $10 \text{ mm}$ —ensure that WSS falls in the range suitable for osteoinduction tests ( $0.1\text{--}20 \text{ dyn cm}^{-2}$ ) (Fernandez-Yague et al., 2015) in a large range of inlet flowrate



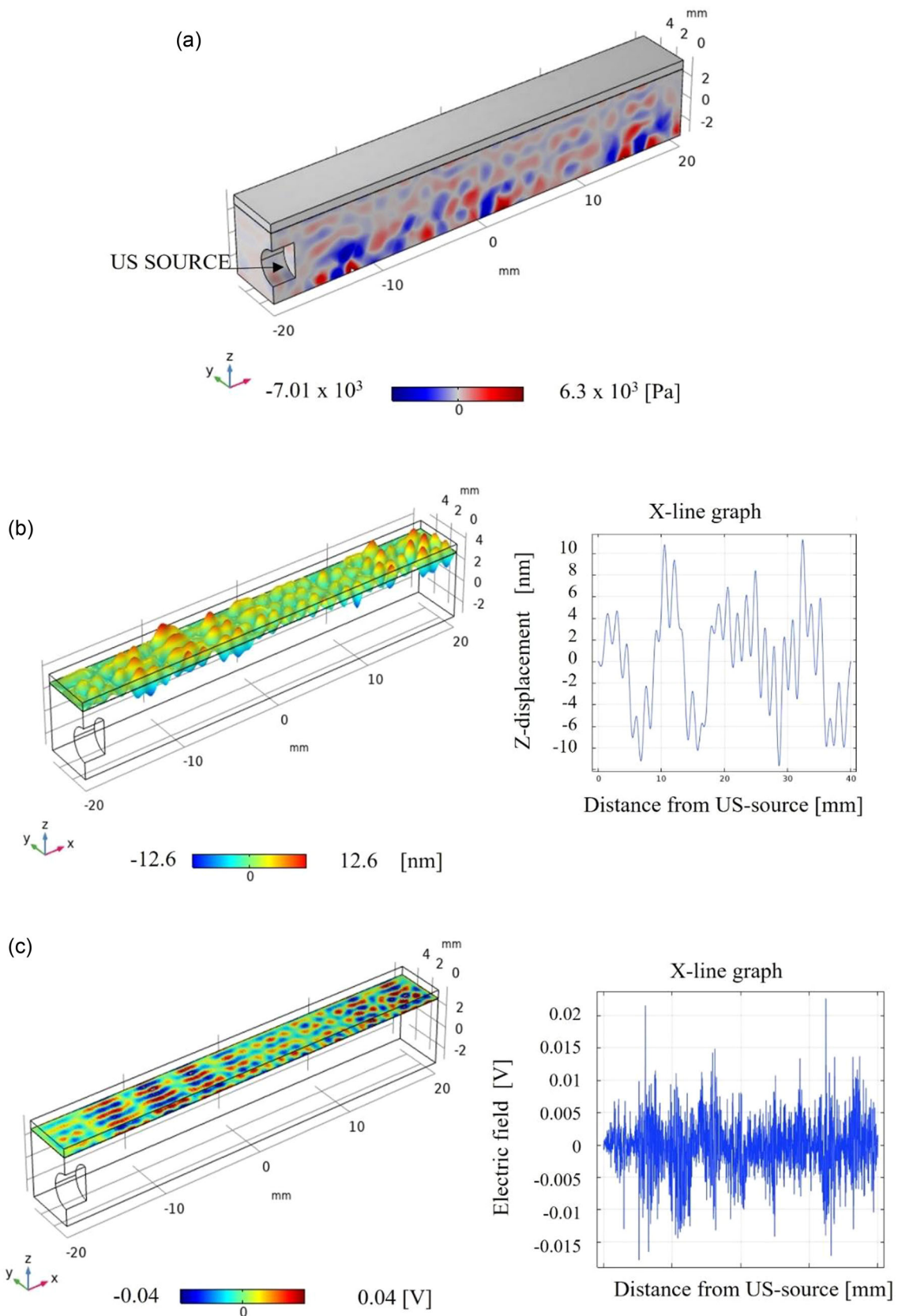


**FIGURE 3** Mechano-acoustic multiphysics simulation of the piezoelectric membrane. The domain symmetry allows to consider just half of the chamber thus reducing the computational demands of the simulation. (a) Acoustic pressure in the bottom compartment with the US-source operating at 2.6 W. (b) Z-displacement above the membrane (nanometer vibration):  $\pm 12$  nm on average. (c) Estimated voltage on the piezoelectric membrane, based on the mechano-acoustic stimulation: 10 mV on average

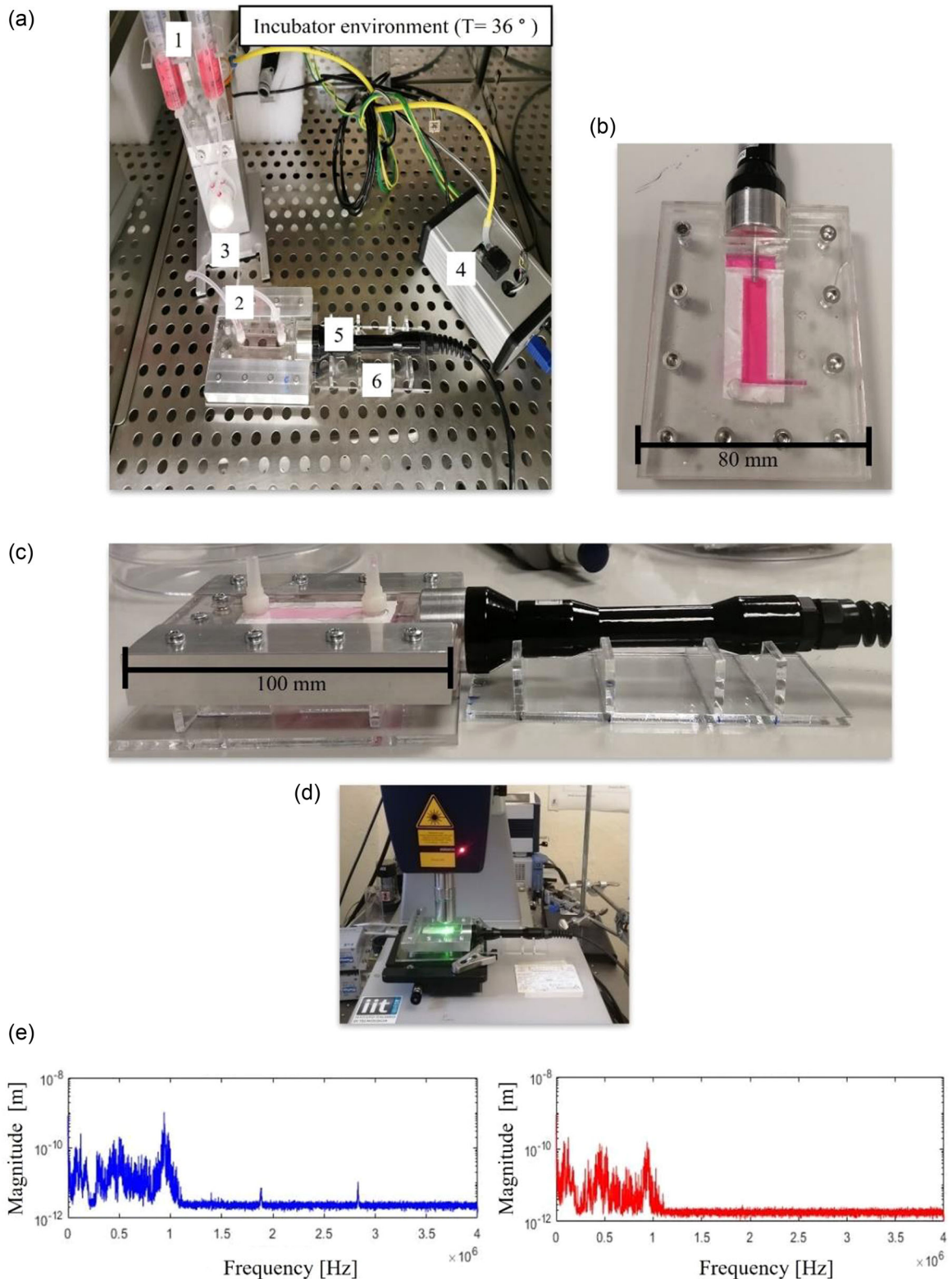


**FIGURE 4** Multimodal bioreactor assembly: (a) Bioreactor inside the incubator during cell adhesion to the substrate, integrated with stimulation systems: (1) medium reservoirs; (2) silicon connecting tubing; (3) peristaltic pump; (4) flow controller; (5) ultrasound planar wave transducer ( $\varnothing_{\text{ext}}$  25 mm,  $\varnothing_{\text{tip}}$  3 mm); (6) transducer support; (out of the incubator) ultrasound generator (SonoPore KTAC-4000). (b) Bottom view of the bioreactor during US probe positioning. (c) Side view of the bioreactor showing the alignment between the probe and the cell culture chamber, ensured by the laser-cut plastic support. (d) Piezoelectric membrane vibrational characterization set-up through laser Doppler vibrometry. (e) Piezoelectric membrane displacement measurements near the US-probe (blue) with a  $D_{\text{rms-NEAR}} = 3$  nm, and vibrations at the end of culture region, far from the US-probe (red) with a  $D_{\text{rms-FAR}} = 1.45$  mm

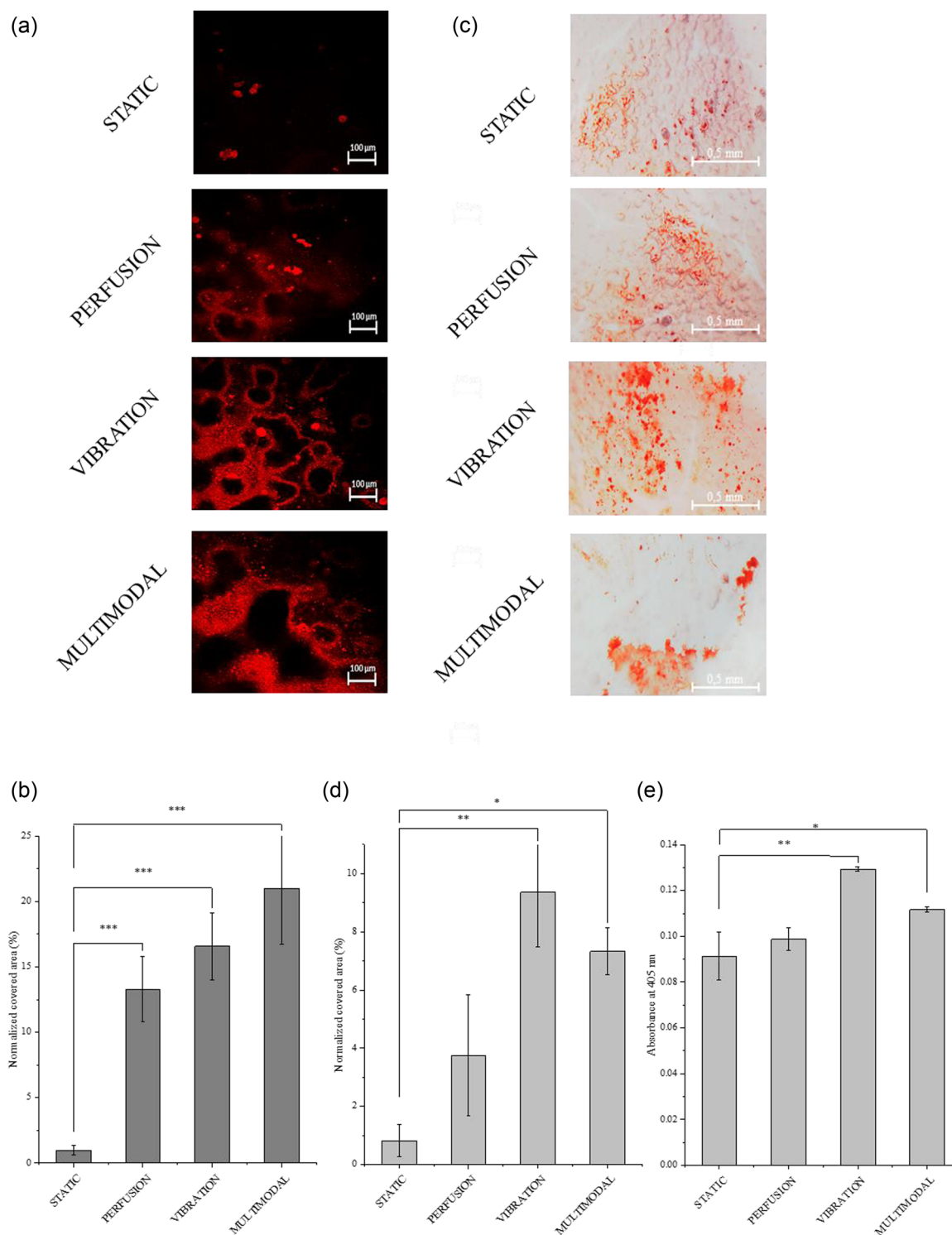


**FIGURE 5** Differentiation evaluation of 7 day-stimulated SaOS-2 cells inside the multimodal and reconfigurable bioreactor: static configuration (no stimuli, control); perfusion-only configuration (flow only, no ultrasound); vibration-only configuration (ultrasound only, no flow); multimodal configuration (flow and ultrasound). (a) Confocal microscopy images of the osteodifferentiation marker collagen-type I (COL-1). (b) COL-1 covered area normalized to total image area (data are presented as mean  $\pm$  SD, \*\*\* $p$  < 0.0001,  $n$  = 3). (c) Optical microscopy images of calcium deposits upon staining with Alizarin Red-S. (d) Calcium deposits covered area normalized to total image area (data are presented as mean  $\pm$  SD, \* $p$  < 0.05, \*\* $p$  < 0.001,  $n$  = 3). (e) Alizarin Red-S quantification through evaluation of the absorbance at 405 nm after dye recovery from samples (data are presented as mean  $\pm$  SD, \* $p$  < 0.05, \*\* $p$  < 0.001,  $n$  = 3)

Also the multimodal configuration induced a significantly higher mineralization with respect to the non-stimulated control (0.11 a.u.). These results once again indicated that the synergic effect of fluidic and electromechanical stimulation could accelerate the differentiation bioprocess of SaOS-2 cells.

## 4 | DISCUSSION

The present work illustrated the development and performances of a novel multimodal biomimetic bioreactor for the *in vitro* osteodifferentiation of human osteoblast-like SaOS-2 cells. The novelty of the proposed multimodal device consists in the possibility to choose whether to implement a hydrodynamic shear stress and nano-scaled mechanical vibrations associated to a wireless electrical impulse—that is, the main physical inputs studied for leading bone cells differentiation (Rangarajan et al., 2014)(Sladkova & de Peppo, 2014)—either in a concomitant and synergistic way, or individually. Which of these stimuli is the main player in the stimulation of osteogenic differentiation is indeed still an open question in the field of BTE; however, what if perhaps there is not a single player, yet the synchronous presence of multiple stimuli working together synergistically toward the optimal outcome?

Numerical multiphysics simulations were carried out to ensure that each physical stimulus is comprised within the range of osteoinduction studies. Precisely, the computed WSS experienced by the piezoelectric substrate should be comprised between 0.7 and 2.1 dyn cm<sup>-2</sup>, by varying the inlet flow rate from 5 to 15 ml min<sup>-1</sup>. These hydrodynamic stress values are considered to be effective in activating the osteogenic response of bone-derived cells without causing detachment from the substrate, as demonstrated by several previous studies. Kreke et al. (2005) exploited a PPFC to exert shear stress on cell monolayers; a value of 1.6 dyn cm<sup>-2</sup> was used for 5, 30, or 120 min a days, on Days 6, 8, 10, and 12 from seeding. Analysis of messenger RNA for bone sialoprotein and osteopontin indicated increased expression of these markers with respect to static cell cultures. In another study conducted by Kapur et al. (2003), a cell culture of human osteoblasts was exposed to steady laminar fluid flow and well-defined fluid shear stress of 20 dyn cm<sup>-2</sup> for 30 min. Again, results of these experimental parameters showed that alkaline phosphatase (Alp) levels were doubled after just 30 min of exposure to shear stress. Similar results were produced by a long-term exposure to shear stresses an order of magnitude lower: in a study conducted by Scaglione et al. (2008), human bone marrow stromal cells were exposed to shear stress of 0.0012 dyn cm<sup>-2</sup> for 10 days using a two-dimensional (2D) parallel plate perfusion system. Even this group assessed that the exposure to shear stress improved the production of calcium and collagen with respect to the static control. Collectively, these studies on short-or long-term exposure to stimulation in 2D cultures indicate that osteogenic is greatly affected by fluid shear stresses with magnitudes as little as 0.001 dyn cm<sup>-2</sup> and as high as 20 dyn cm<sup>-2</sup>.

Mechanical stimulation delivered through high frequency nanometer vibrations has been already investigated to induce osteogenesis, exploiting different combination of vibration parameters. Nikukar et al. used nanoscale sinusoidal mechanotransductive protocols (10–14 nm displacements at 500 and 1000 Hz frequency) to promote osteoblastogenesis in human mesenchymal stem cells (hMSCs) (Nikukar et al., 2013). It resulted that bone morphogenic protein 2 expression greatly increased in response to 1 kHz stimulation but not 500 Hz after 24 h of culture. Also, runt-related transcription factor 2 expression—responsible for transcription and thus expression of bone-related protein such as osteocalcin—did not change between control and 500 Hz stimulation, but showed upregulation after 1 kHz stimulation for 1 week. This was confirmed by osteocalcin expression after 14 days, increased in response to 1 kHz stimulation compared to control and to 500 Hz. These results set the stage for a deeper investigation of nanoscale vibrations to activate osteogenic pathway, instead of the traditional application of macroscopic strain/compression to cell/material constructs. Two years later, the same group (Pemberton et al., 2015) exploited nano vibrations at higher frequencies (1–5 kHz) and higher vertical displacement (16–30 nm) by using a standard piezo-actuator. It resulted into the upregulation of osteoblastic genes and in a more abundant deposition of calcium phosphate, at all the tested frequencies (1, 3, and 5 kHz) with respect to not stimulated control, but it was noted that the 5 kHz stimulation induced the highest expression of markers. Again, these results shows that high-frequency vertical nano displacements can have a large effect on the development of the osteoblast phenotype. In all the above mentioned studies, scientists pointed out that increasing the delivered vibration frequency, along decreasing the vertical displacement value to the order of cell focal adhesions, could have greater effects on osteodifferentiation. In our study, we thus investigated this hypothesis, developing a vibrational set up reaching an amplitude of ~12 nm with a frequency of 1 MHz. This amplitude vibration on membrane surface is induced by an immersion ultrasound probe at its maximum power ~2.6 W and frequency ~1 MHz. We can not directly compare our results with the previous ones because of discrepancies between adopted biological assay and type of cells, but we have also verified an increment of collagen expression and of calcium deposit in the nano vibrational stimulated sample with respect to the control. It should also be specified that the vibration of the piezoelectric membrane lead the development of an electrical potential of ~10 mV, that could be the predominant stimulus to the resulting cell differentiation. In a future study, the testing of the effect of vibration alone, by replacing the piezoelectric membrane with a standard nonpiezoelectric substrate, would be worth of investigation, so as to dissociate the two stimuli and evaluate the prevalent one.

Indeed, also electrical and electromagnetic stimulation (EMS) has been shown to be efficient in bone regeneration (Nikukar et al., 2013). Although the detailed electro-transduction mechanisms underlying osteodifferentiation are still poorly understood, asymmetric redistribution/diffusion of electrically charged cell membrane receptors or direct activation of voltage-gated Ca<sup>2+</sup> channels, which



further activate numerous downstream signaling cascades (Leppik et al., 2020), are believed to be at the base of osteodifferentiation. Alongside traditional EMS methods based on invasive electrodes (DC, PEMF, CC), the use of piezoelectric materials is becoming increasingly popular, as they could combine scaffoldings and electromechanical stimulation into a single device, offering precise control over the amount, duration, and localization of the stimulus, as well as a noninvasive electric stimulation approach. Many piezoelectric materials have been tested to promote osteoregeneration both in vitro and in vivo. In a study of our group, "Osteo-prints" (OP) scaffolds have been doped with BTNPs to further promote and enhance osteogenic differentiation by combining topographic with piezoelectric stimulation with respect to undoped substrates (Marino et al., 2015). In a more recent study, still from our group, BNNTs were used as second phase reinforcing agent of a P(VDF-TrFE) piezoelectric films. SaOS-2 cells were used to assess biological osteogenic effect of the US-activated piezoelectric nanocomposite films, that generated a surface voltage of 20–60 mV (Genchi et al., 2018). Results showed that transcriptional levels of osteogenic differentiation markers, for example, Alp, Col1 $\alpha$ 1, Integrin binding sialoprotein, and osteonectin were significantly higher in cells cultured on nanocomposite films and exposed to US with respects to relevant controls. All together, these results indicate that combining a mechanical stimulus with a piezoelectric one could induce a significant osteogenic enhancement; this is in agreement with the well-known fact that bone constituents, particularly collagen, possess an intrinsic piezoelectricity that could have a significant bearing on the osteoregeneration process (Fukada, 2016) (Rajabi et al., 2015).

The integration of these three stimuli—the hydrodynamic shear stress, the nano-scaled substrate vibration, and the low intensity localized electric voltage—within a single bioreactor, leak-free, easy to be assembled and handled, as well as completely transparent, open intriguing perspectives toward a clearer elucidation of which are the actors in the osteogenic mechano-transduction. We found that shear stress and electroactive nanoscale vibration effectively enhance the process of osteogenic differentiation with respect to the static control, but the most significant result was obtained by simultaneously combining these stimuli in the multimodal configuration. The easy tunability of the integrated biomimetic system paves the way to the possibility of exploring different experimental set-up, for example increasing US power and thus electric output generation, or varying the flow rate and thus the hydrodynamic stress on the cell culture; integration of 3D culture approaches would be finally a relevant improvement of our platform.

## 5 | CONCLUSION

To conclude, the presented bioreactor could represent a novel cell culturing and stimulating device, reconfigurable and adaptable for many applications, that could bring a great contribution to the knowledge of mechanotransduction/electrotransduction phenomena in several fields of tissue engineering, integrating many of its features

into a single user-friendly device. Further ameliorations of the developed bioreactor may consist in the insertion of a second ultrasound transducer, on the opposite side of the first one and along the same axis in the chamber, to guarantee a more spatially uniform and powerful vibrational stimulation. By taking into consideration the multimodal operability of the device and the easy fabrication of its fluidic cell culture chamber, our bioreactor would be suitable for culturing of different cell types, such muscle cells due to their electrical and mechanical responsiveness, by modifying stimulation parameters and the flow chamber in shape and size.

## ACKNOWLEDGMENTS

We gratefully acknowledge Dr. Matteo Battaglini (Istituto Italiano di Tecnologia, Italy) for technical assistance at confocal microscopy. Open Access Funding provided by Istituto Italiano di Tecnologia within the CRUI-CARE Agreement.

## CONFLICTS OF INTEREST

The authors declare no conflicts of interest.

## DATA AVAILABILITY STATEMENT

The data that support the findings of this study are available from the corresponding author upon reasonable request.

## ORCID

Margherita Montorsi  <http://orcid.org/0000-0003-3916-2966>

Gianni Ciofani  <http://orcid.org/0000-0003-1192-3647>

## REFERENCES

- Benya, P. D., Kavanaugh, A., Zakarian, M., Söderlind, P., Jashashvili, T., Zhang, N., Waldorff, E. I., Ryaby, J. T., & Billi, F. (2021). Pulsed electromagnetic field (PEMF) transiently stimulates the rate of mineralization in a 3-dimensional ring culture model of osteogenesis. *PLOS One*, 16(2), e0244223.
- Bhavsar, M. B., Han, Z., DeCoster, T., Leppik, L., Oliveira, K. M. C., & Barker, J. H. (2020). Electrical stimulation-based bone fracture treatment, if it works so well why do not more surgeons use it? *European Journal of Trauma and Emergency Surgery*, 46(2), 245–264.
- Braddock, M., Houston, P., Campbell, C., & Ashcroft, P. (2001). Born again bone: Tissue engineering for bone repair. *Physiology*, 16(5), 208–213.
- Cafarelli, A., Verbeni, A., Poliziani, A., Dario, P., Menciassi, A., & Ricotti, L. (2017). Tuning acoustic and mechanical properties of materials for ultrasound phantoms and smart substrates for cell cultures. *Acta Biomaterialia*, 49, 368–378.
- Campsie, P., Childs, P. G., Robertson, S. N., Cameron, K., Hough, J., Salmeron-Sanchez, M., Tsimbouri, P. M., Vichare, P., Dalby, M. J., & Reid, S. (2019). Design, construction and characterisation of a novel nanovibrational bioreactor and cultureware for osteogenesis. *Scientific Reports*, 9(1), 1–12.
- Castro, N., Ribeiro, S., Fernandes, M. M., Ribeiro, C., Cardoso, V., Correia, V., Minguez, R., & Lanceros-Mendez, S. (2020). Physically active bioreactors for tissue engineering applications. *Advanced Biosystems*, 4(10), 2000125.
- Chalidis, B., Sachinis, N., Assiotis, A., Maccauro, G., & Graziani, F. (2011). Stimulation of bone formation and fracture healing with pulsed electromagnetic fields: Biologic responses and clinical implications. *International Journal of Immunopathology and Pharmacology*, 24(1\_suppl2), 17–20.



- Chiu, C. Y., Tsai, T. L., Vanderby, R., Jr., Bradica, G., Lou, S. L., & Li, W. J. (2015). Osteoblastogenesis of mesenchymal stem cells in 3-D culture enhanced by low-intensity pulsed ultrasound through soluble receptor activator of nuclear factor kappa B ligand. *Ultrasound in Medicine & Biology*, *41*(7), 1842–18.
- Choi, H. S., Lee, W. J., & Jung, J. T. (2019). *U.S. Patent No. 10,260,035*. Patent and Trademark Office.
- Ciofani, G., Danti, S., Genchi, G. G., Mazzolai, B., & Mattoli, V. (2013). Boron nitride nanotubes: Biocompatibility and potential spill-over in nanomedicine. *Small*, *9*(9–10), 1672–1685.
- Coelho, M. J., & Fernandes, M. H. (2000). Human bone cell cultures in biocompatibility testing. Part II: Effect of ascorbic acid,  $\beta$ -glycerophosphate and dexamethasone on osteoblastic differentiation. *Biomaterials*, *21*(11), 1095–1102.
- Curtis, A. S., Reid, S., Martin, I., Vaidyanathan, R., Smith, C. A., Nikukar, H., & Dalby, M. J. (2013). Cell interactions at the nanoscale: Piezoelectric stimulation. *IEEE Transactions on Nanobioscience*, *12*(3), 247–254.
- Dalby, M. J., Andar, A., Nag, A., Affrossman, S., Tare, R., McFarlane, S., & Oreffo, R. O. (2008). Genomic expression of mesenchymal stem cells to altered nanoscale topographies. *Journal of the Royal Society Interface*, *5*(26), 1055–1065.
- Diniz, P., Shomura, K., Soejima, K., & Ito, G. (2002). Effects of pulsed electromagnetic field (PEMF) stimulation on bone tissue like formation are dependent on the maturation stages of the osteoblasts. *Bioelectromagnetics*, *23*(5), 398–405.
- Dong, Y., Suryani, L., Zhou, X., Muthukumaran, P., Rakshit, M., Yang, F., Wen, F., Hassanbhai, A. M., Parida, K., Simon, D. T., landolo, D., Lee, P. S., Ng, K. W., & Teoh, S. H. (2021). Synergistic effect of PVDF-coated PCL-TCP scaffolds and pulsed electromagnetic field on osteogenesis. *International Journal of Molecular Sciences*, *22*(12), 6438.
- Fernandez-Yague, M. A., Abbah, S. A., McNamara, L., Zeugolis, D. I., Pandit, A., & Biggs, M. J. (2015). Biomimetic approaches in bone tissue engineering: Integrating biological and physicochemical strategies. *Advanced Drug Delivery Reviews*, *84*, 1–29.
- Fukada, E. (2016). Piezoelectricity and electrostimulation in bone. *Electrically Active Materials for Medical Devices*, *2*, 19–28.
- Genchi, G. G., Ceseracciu, L., Marino, A., Labardi, M., Marras, S., Pignatelli, F., Bruschini, L., Mattoli, V., & Ciofani, G. (2016). P(VDF-TrFE)/BaTiO<sub>3</sub> nanoparticle composite films mediate piezoelectric stimulation and promote differentiation of SH-SY5Y neuroblastoma cells. *Advanced Healthcare Materials*, *5*(14), 1808–1820.
- Genchi, G. G., Sinibaldi, E., Ceseracciu, L., Labardi, M., Marino, A., Marras, S., De Simoni, G., Mattoli, V., & Ciofani, G. (2018). Ultrasound-activated piezoelectric P(VDF-TrFE)/boron nitride nanotube composite films promote differentiation of human SaOS-2 osteoblast-like cells. *Nanomedicine: Nanotechnology, Biology, and Medicine*, *14*(7), 2421–2432.
- Goldstein, A. S., Juarez, T. M., Helmke, C. D., Gustin, M. C., & Mikos, A. G. (2001). Effect of convection on osteoblastic cell growth and function in biodegradable polymer foam scaffolds. *Biomaterials*, *22*(11), 1279–1288.
- Grillone, A., Battaglini, M., Moscato, S., Mattii, L., De Julián Fernández, C., Scarpellini, A., Giorgi, M., Sinibaldi, E., & Ciofani, G. (2019). Nutlin-loaded magnetic solid lipid nanoparticles for targeted glioblastoma treatment. *Nanomedicine*, *14*(6), 727–752.
- Hadida, M., & Marchat, D. (2020). Strategy for achieving standardized bone models. *Biotechnology and Bioengineering*, *117*(1), 251–271.
- Ingber, D. E., Benam, K. H., Villenave, R., Hamilton, G. A., Hassell, B., Hinojosa, C. D., & Lucchesi, C. (2021). *U.S. Patent No. 11,119,093*. Patent and Trademark Office.
- Kapur, S., Baylink, D. J., & Lau, K. H. W. (2003). Fluid flow shear stress stimulates human osteoblast proliferation and differentiation through multiple interacting and competing signal transduction pathways. *Bone*, *32*(3), 241–251.
- Katsumi, A., Orr, A. W., Tzima, E., & Schwartz, M. A. (2004). Integrins in mechanotransduction. *Journal of Biological Chemistry*, *279*(13), 12001–12004.
- Khaw, J. S., Xue, R., Cassidy, N. J., & Cartmell, S. H. (2021). Electrical stimulation of titanium to promote stem cell orientation, elongation and osteogenesis. *Acta Biomaterialia*, *139*, 204–217.
- Kilian, K. A., Bugarija, B., Lahn, B. T., & Mrksich, M. (2010). Geometric cues for directing the differentiation of mesenchymal stem cells. *Proceedings of the National Academy of Sciences*, *107*(11), 4872–4877.
- Kim, I. S., Song, Y. M., Lee, B., & Hwang, S. J. (2012). Human mesenchymal stromal cells are mechanosensitive to vibration stimuli. *Journal of Dental Research*, *91*(12), 1135–1140.
- Kreke, M. R., Huckle, W. R., & Goldstein, A. S. (2005). Fluid flow stimulates expression of osteopontin and bone sialoprotein by bone marrow stromal cells in a temporally dependent manner. *Bone*, *36*(6), 1047–1055.
- Kreke, M. R., Sharp, L. A., Woo Lee, Y., & Goldstein, A. S. (2008). Effect of intermittent shear stress on mechanotransductive signaling and osteoblastic differentiation of bone marrow stromal cells. *Tissue Engineering Part A*, *14*(4), 529–537.
- Langenbach, F., & Handschel, J. (2013). Effects of dexamethasone, ascorbic acid and  $\beta$ -glycerophosphate on the osteogenic differentiation of stem cells in vitro. *Stem Cell Research & Therapy*, *4*(5), 1–7.
- Leppik, L., Oliveira, K. M. C., Bhavsar, M. B., & Barker, J. H. (2020). Electrical stimulation in bone tissue engineering treatments. *European Journal of Trauma and Emergency Surgery*, *46*, 1–14.
- Liu, B., Han, S., Modarres-Sadeghi, Y., & Lynch, M. E. (2021). Multiphysics simulation of a compression-perfusion combined bioreactor to predict the mechanical microenvironment during bone metastatic breast cancer loading experiments. *Biotechnology and Bioengineering*, *118*(5), 1779–1792.
- Liu, J., Zhao, Z., Li, J., Zou, L., Shuler, C., Zou, Y., Huang, X., Li, M., & Wang, J. (2009). Hydrostatic pressures promote initial osteodifferentiation with ERK1/2 not p38 MAPK signaling involved. *Journal of Cellular Biochemistry*, *107*(2), 224–232.
- Marino, A., Genchi, G. G., Sinibaldi, E., & Ciofani, G. (2017). Piezoelectric effects of materials on bio-interfaces. *ACS Applied Materials & Interfaces*, *9*(21), 17663–17680.
- Marino, A., Filippeschi, C., Genchi, G. G., Mattoli, V., Mazzolai, B., & Ciofani, G. (2014). The Osteoprint: A bioinspired two-photon polymerized 3-D structure for the enhancement of bone-like cell differentiation. *Acta Biomaterialia*, *10*(10), 4304–4313.
- Marino, A., Barsotti, J., de Vito, G., Filippeschi, C., Mazzolai, B., Piazza, V., Labardi, M., Mattoli, V., & Ciofani, G. (2015). Two-photon lithography of 3D nanocomposite piezoelectric scaffolds for cell stimulation. *ACS Applied Materials & Interfaces*, *7*(46), 25574–25579.
- Martin, I., Wendt, D., & Heberer, M. (2004). The role of bioreactors in tissue engineering. *Trends in Biotechnology*, *22*(2), 80–86.
- McCoy, R. J., & O'Brien, F. J. (2010). Influence of shear stress in perfusion bioreactor cultures for the development of three-dimensional bone tissue constructs: A review. *Tissue Engineering Part B: Reviews*, *16*(6), 587–601.
- Meneses, J., C. Silva, J., R. Fernandes, S., Datta, A., Castelo Ferreira, F., Moura, C., Amado, S., Alves, N., & Pascoal-Faria, P. (2020). A multimodal stimulation cell culture bioreactor for tissue engineering: A numerical modelling approach. *Polymers*, *12*(4), 940.
- Navarro, J., Swayambunathan, J., Janes, M. E., Santoro, M., Mikos, A. G., & Fisher, J. P. (2019). Dual-chambered membrane bioreactor for coculture of stratified cell populations. *Biotechnology and Bioengineering*, *116*(12), 3253–3268.

- Nikukar, H., Reid, S., Tsimbouri, P. M., Riehle, M. O., Curtis, A. S., & Dalby, M. J. (2013). Osteogenesis of mesenchymal stem cells by nanoscale mechanotransduction. *ACS Nano*, 7(3), 2758–2767.
- Pemberton, G. D., Childs, P., Reid, S., Nikukar, H., Tsimbouri, P. M., Gadegaard, N., Curtis, A. S., & Dalby, M. J. (2015). Nanoscale stimulation of osteoblastogenesis from mesenchymal stem cells: Nanotopography and nanokicking. *Nanomedicine*, 10(4), 547–560.
- Ponomarenko, M. A. (2016). U.S. Patent Application No. 15/101,861.
- Prodanov, L., van Loon, J. J., te Riet, J., Jansen, J. A., & Walboomers, X. F. (2013). Substrate nanotexture and hypergravity through centrifugation enhance initial osteoblastogenesis. *Tissue Engineering Part A*, 19(1-2), 114–124.
- Rajabi, A. H., Jaffe, M., & Arinze, T. L. (2015). Piezoelectric materials for tissue regeneration: A review. *Acta Biomaterialia*, 24, 12–23.
- Rangarajan, S., Madden, L., & Bursac, N. (2014). Use of flow, electrical, and mechanical stimulation to promote engineering of striated muscles. *Annals of Biomedical Engineering*, 42(7), 1391–1405.
- Ravichandran, A., Wen, F., Lim, J., Chong, M. S. K., Chan, J. K., & Teoh, S. H. (2018). Biomimetic fetal rotation bioreactor for engineering bone tissues—Effect of cyclic strains on upregulation of osteogenic gene expression. *Journal of Tissue Engineering and Regenerative Medicine*, 12(4), e2039–e2050.
- Ribeiro, C., Pärssinen, J., Sencadas, V., Correia, V., Miettinen, S., Hytönen, V. P., & Lanceros-Méndez, S. (2015). Dynamic piezoelectric stimulation enhances osteogenic differentiation of human adipose stem cells. *Journal of Biomedical Materials Research Part A*, 103(6), 2172–2175.
- Scaglione, S., Wendt, D., Miggino, S., Papadimitropoulos, A., Fato, M., Quarto, R., & Martin, I. (2008). Effects of fluid flow and calcium phosphate coating on human bone marrow stromal cells cultured in a defined 2D model system. *Journal of Biomedical Materials Research Part A*, 86(2), 411–419.
- Sladkova, M., & de Peppo, G. M. (2014). Bioreactor systems for human bone tissue engineering. *Processes*, 2(2), 494–525.
- Srirussamee, K., Xue, R., Mobini, S., Cassidy, N. J., & Cartmell, S. H. (2021). Changes in the extracellular microenvironment and osteogenic responses of mesenchymal stem/stromal cells induced by in vitro direct electrical stimulation. *Journal of Tissue Engineering*, 12, 2041731420974147.
- Stewart, S., Darwood, A., Masouros, S., Higgins, C., & Ramasamy, A. (2020). Mechanotransduction in osteogenesis. *Bone & Joint Research*, 9(1), 1–14.
- Surmenev, R. A., Orlova, T., Chernozem, R. V., Ivanova, A. A., Bartasyte, A., Mathur, S., & Surmeneva, M. A. (2019). Hybrid lead-free polymer-based nanocomposites with improved piezoelectric response for biomedical energy-harvesting applications: A review. *Nano Energy*, 62, 475–506.
- Suzuki, A., Takayama, T., Suzuki, N., Sato, M., Fukuda, T., & Ito, K. (2009). Daily low-intensity pulsed ultrasound-mediated osteogenic differentiation in rat osteoblasts. *Acta Biochimica et Biophysica Sinica*, 41(2), 108–115.
- Teoh, S. H., Chua, P. H., Ravichandran, A., Chong, W. S., Wen, F., Hassanbhai, A. M., & Suryani, L. (2021). U.S. Patent Application No. 16/477,861.
- Uddin, S. M., & Qin, Y. X. (2013). Enhancement of osteogenic differentiation and proliferation in human mesenchymal stem cells by a modified low intensity ultrasound stimulation under simulated microgravity. *PLoS One*, 8(9), e73914.
- Van Dyke, W. S., Sun, X., Richard, A. B., Nauman, E. A., & Akkus, O. (2012). Novel mechanical bioreactor for concomitant fluid shear stress and substrate strain. *Journal of Biomechanics*, 45(7), 1323–1327.
- Yeatts, A. B., & Fisher, J. P. (2011). Bone tissue engineering bioreactors: Dynamic culture and the influence of shear stress. *Bone*, 48(2), 171–181.
- Zeuner, M. T., Didenko, N. N., Humphries, D., Stergiadis, S., Morash, T. M., Patel, K., Grimm, W. D., & Wüder, D. (2018). Isolation and characterization of neural crest-derived stem cells from adult ovine palatal tissue. *Frontiers in Cell and Developmental Biology*, 6, 39.
- Zhang, X., Zhang, C., Lin, Y., Hu, P., Shen, Y., Wang, K., Meng, S., Chai, Y., Dai, X., Liu, X., Liu, Y., Mo, X., Cao, C., Li, S., Deng, X., & Chen, L. (2016). Nanocomposite membranes enhance bone regeneration through restoring physiological electric microenvironment. *ACS Nano*, 10(8), 7279–7286.
- Zhang, Y., Xu, L., Liu, Z., Cui, X., Xiang, Z., Bai, J., Jiang, D., Xue, J., Wang, C., Lin, Y., Li, Z., Shan, Y., Yang, Y., Bo, L., Li, Z., & Zhou, X. (2021). Self-powered pulsed direct current stimulation system for enhancing osteogenesis in MC3T3-E1. *Nano Energy*, 85, 106009.

## SUPPORTING INFORMATION

Additional supporting information can be found online in the Supporting Information section at the end of this article.

**How to cite this article:** Montorsi, M., Genchi, G. G., De Pasquale, D., De Simoni, G., Sinibaldi, E., & Ciofani, G. (2022). Design, fabrication, and characterization of a multimodal reconfigurable bioreactor for bone tissue engineering. *Biotechnology and Bioengineering*, 119, 1965–1979. <https://doi.org/10.1002/bit.28100>